GRAPHENE FOAM/CONDUCTIVE POLYMER COMPOSITES FOR LIGHTWEIGHT ELECTROMAGNETIC INTERFERENCE SHIELDING

Ying Wu[1]*, Zhenyu Wang[1], Xu Liu[1], Xi Shen[1], Qingbin Zheng[1], and Jang-Kyo Kim[1]

[1] Department of Mechanical and Aerospace Engineering, The Hong Kong University of Science and Technology, Kowloon, Hong Kong
* Corresponding author (ywubb@connect.ust.hk)

Keywords: Graphene foam composites, Ultralightweight, Electrical conductivity, EMI shielding

ABSTRACT

This paper presents our recent work [1] on developing a novel and facile strategy for the fabrication of highly conductive and lightweight graphene foam (GF)/poly(3,4-ethylenedioxythiophene): poly(styrenesulfonate) (PEDOT:PSS) composites for effective electromagnetic interference (EMI) shielding. The surfactant, 4-dodecylbenzenesulfonic acid, is applied for noncovalent functionalization of cellular-structured, freestanding GFs to enhance the wettability and the interfacial interactions between GFs and PEDOT:PSS and thus help coat PEDOT:PSS on GFs. A uniform and highly porous structure is developed, showing a high porosity of 98.8% and a low density of 18.2×10^{-3} g/cm^3. A much enhanced electrical conductivity from 11.8 to 43.2 S/cm is achieved and discussion is made of interfacial interactions and physical/morphological changes on both the microscopic and nanoscopic scales. The highly conductive PEDOT:PSS coating bridges resistive grain boundaries and connects open areas of the cellular structure of GFs. Negative permittivities and permeabilities are observed for the composites, an indication of charge delocalization at the interfaces of PEDOT:PSS and GFs on a microscopic scale. Thanks to the lightweight porous structure, excellent electrical conductivities and effective charge delocalization, the GF/PEDOT:PSS composites deliver exceptional EMI shielding performances with a shielding effectiveness (SE) of 91.9 dB and specific SEs of 3124 dB·cm^3/g and 20800 dB·cm^2/g normalized by volumetric and area densities, respectively. These excellent EMI shielding performances are among the best of reported values for different composites. The remarkable EMI shielding properties and proposed mechanisms in this work can shed new insights into how one can improve EMI shielding performance.

1 INTRODUCTION

The fast-developing and extensive use of electronics has inevitably generated severe electromagnetic (EM) pollutions that are detrimental to both the normal operation of electronics and the health of human being. Therefore, it is increasingly important to develop effective EM interference (EMI) shielding materials to reduce the emanation of EM waves in free spaces and to protect neighboring components in electronics. Excellent EMI shielding properties and lightweights are critical requirements for applications in emerging areas, such as aircraft, aerospace and automobiles. Generally, two strategies are explored for the fabrication of lightweight EMI shielding materials: (i) the construction of porous structures, and (ii) the application of polymer composites reinforced with highly conductive fillers, especially graphene and carbon nanotubes (CNTs) [2-4]. Apart from the reduction of material density, porous structures contribute to the improvement of EMI shielding performance by enhancing multiple reflection of EM waves within the material. The incorporation of highly conductive fillers improve the interactions between EM radiation and shielding materials, which is also beneficial to EMI shielding.

Among different polymer composites reinforced with conductive fillers, graphene/polymer composites are the most promising for superior EMI shielding because of excellent electrical conductivities, large specific surface areas, and large electron mobility of graphene fillers. Graphene foams (GFs) with a continuous cellular structure are popular fillers for the fabrication of porous

polymer-based composites with great electrical and EMI shielding properties [4, 5]. An ultrahigh EMI shielding effectiveness (SE) of ~75 dB and a large specific SE (SSE, SE normalized by volumetric density) of ~833 dB·cm^3/g were reported for GF/CNT/polydimethylsiloxane (PDMS) composites [4]. The widely used matrices for the fabrication of polymer composites for EMI shielding applications are nonconductive polymers, such as PDMS, polystyrene (PS), epoxy, and poly(vinylidene fluoride) (PVDF). With extremely low SE values of generally smaller than 1 dB, nonconductive polymers are transparent to EM waves [6, 7]. As an alternative, conducting polymers, such as polypyrrole, polyaniline, and poly(3,4-ethylenedioxythiophene):poly(styrenesulfonate) (PEDOT:PSS), are found to be effective in enhancing EMI shielding performance due to their high electrical conductivities and non-transparency to EM radiations [8-10].

In order to develop EMI shielding materials with high electrical conductivities, lightweight and easy processing, GF/PEDOT:PSS composites are produced by drop coating PEDOT:PSS aqueous solutions on 4-dodecylbenzenesulfonic acid (DBSA) functionalized freestanding GFs. A uniform, porous structure with a high porosity of 98.8% and an ultralow density of 18.2×10^{-3} g/cm^3 is obtained. Excellent electrical conductivities as high as 43.2 S/cm and extraordinary EMI SE of over 90 dB were achieved. The mechanisms behind the outstanding EMI shielding of the composites are proposed based on experimental and theoretical analyses.

2 EXPERIMENTAL

2.1 Composites synthesis

GFs were prepared using chemical vapor deposition method [11, 12] by applying a 500 standard cubic centimetre per minute (sccm) of Ar, 200 sccm of H_2, and a concentration of 2.8 vol% of CH_4. The carbon deposition temperature and time were 1000 ºC and 20 min, respectively, after an annealing of 10 min at 1000 ºC. After the etching of the Ni substrate, DBSA was applied on freestanding GFs, which was denoted as DBSA@GF, for noncovalent functionalization to enhance the wettability and interactions between GFs and PEDOT:PSS. The PEDOT:PSS aqueous solution (CLEVIOS PH 1000) was added with 5 vol % dimethyl sulfoxide (DMSO, Sigma-Aldrich, anhydrous) and then diluted to half its original concentration using deionized water. The mixture was then drop coated on DBSA@GF, followed by drying at 80 ºC for 0.5 h. The schematic procedure for the fabrication of GF/PEDOT:PSS composites is illustrated in Figure 1a. Composites with different PEDOT:PSS-to-GF weight ratio were fabricated by depositing different amount of consecutive coatings and were expressed as GF/PEDOT:PSS-X.

2.2 Characterization

Morphologies of GFs and GF/PEDOT:PSS were observed by scanning electron microscope (SEM, JEOL JSM 6390). Wettability of DBSA@GFs obtained by applying different concentration of DBSA solutions was observed by a goniometer (Kruss G10 Contact Angle Measuring System) using compressed GFs as the target material. Ultraviolet−visible (UV−vis) spectroscopy (PerkinElmer Lambda 20) and Fourier transform infrared spectroscopy (FT-IR, Bruker Vertex 70 Hyperion 1000) were used to identify interfacial interactions between GFs, DBSA and PEDOT:PSS. The electrical conductivities were measured by the four-point probe method (Scientific Equipment & Services). Porosities were calculated according to Eq (1) [12] with densities of graphene and PEDOT:PSS being 2.2 and 1 g/cm^3, respectively:

$$\beta = \left(1-\rho_a/\rho_t\right)\times 100\% \tag{1}$$

where ρ_a and ρ_t are the apparent and the true densities of composites. The scattering parameters, S_{11} and S_{21}, in the range of 8-12 GHz were measured via waveguide transmission line method by a vector network analyzer (Agilent Technologies N5230A). EMI SEs attributed to absorption (SE_A), reflection (SE_R), and the total SE (SE_T) were evaluated by Eq (2-4) [4]:

$$SE_A(dB) = -10\log\left[S_{21}{}^2/\left(1-S_{11}{}^2\right)\right] \tag{2}$$

$$SE_R(dB) = -10\log\left(1 - S_{11}{}^2\right) \tag{3}$$

$$SE_T(dB) = SE_A + SE_R \tag{4}$$

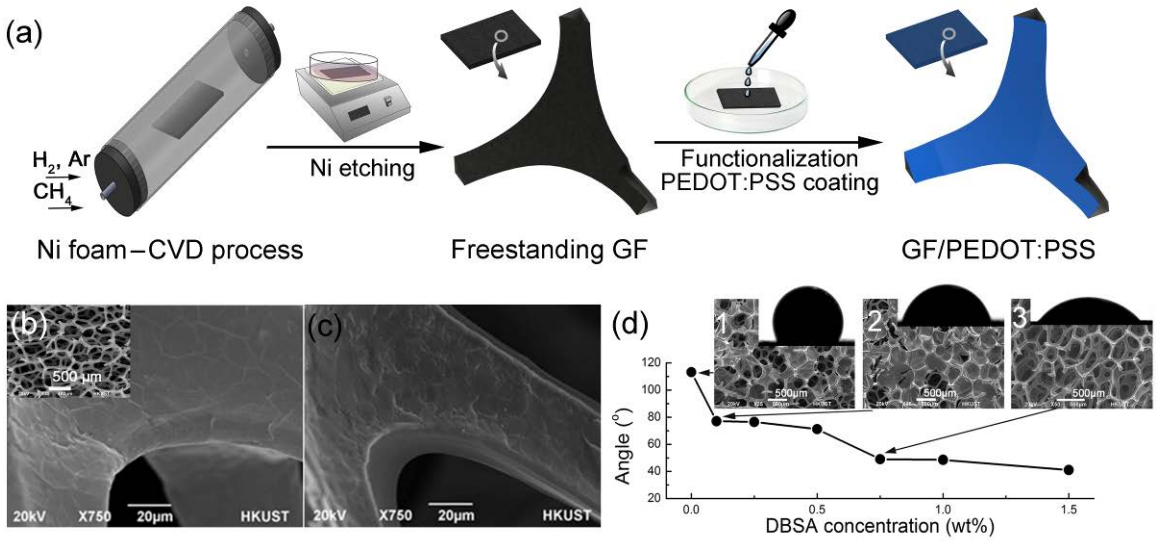

Figure 1: (a) Schematics of the synthesis of GF/PEDOT:PSS composites; SEM images of (b) freestanding GFs, and (c) GF/PEDOT:PSS; and (d) contact angles measured on compressed DBSA@GFs as a function of DBSA concentration. Insets in (d) show the SEM images of GF/PEDOT:PSS composites and images of PEDOT:PSS droplets on target materials functionalized by different DBSA concentrations.

3 RESULTS AND DISCUSSION

3.1 Characteristics of GFs and GF/PEDOT:PSS Composites.

GFs possess a cellular porous structure with wrinkles (Figure 1b) resulted from grain boundaries of the Ni foam templates. The as-prepared freestanding GFs is incompatible with PEDOT:PSS aqueous solutions because of their hydrophobicity arising from the absence of hydrophilic functional groups. Upon applying PEDOT:PSS solutions, the GFs showed a very large contact angle of 113º and a detachment of the polymer coating (inset 1 in Figure 1d). After the DBSA functionalization, contact angles gradually decreased, indicating enhanced wettability of GFs. The functionalization using 0.75 wt% DBSA solution guaranteed a full penetration of PEDOT:PSS solution into GFs and led to a uniform polymer coating (Figure 1c,d). Considering the conductive nature of DBSA, 0.75 wt% DBSA aqueous solution was used for the preparation of composites.

Interfacial interactions among GF, DBSA and PEDOT:PSS were examined by UV−vis, Raman, and FT-IR. The UV−vis peak (Figure 2a) located at 269 nm is a suggestion of phenyl groups of graphene. After the functionalization, the peak underwent a 3-nm shift to 271 nm, indicating the formation of π−π stacking interactions between DBSA and graphene. The Raman spectrum of the as-prepared GFs (Figure 2b) shows G- and 2D-band peaks located at ~1580 and ~2700 cm^{-1}, respectively. The absence of D-band centered at ~1350 cm^{-1} is attributed to the perfect graphitic structure, resulting in the high hydrophilicity and large electrical conductivity which will be discussed below. After the DBSA functionalization, the G-band peak of GFs up-shifted from 1579 to 1582 cm^{-1} (as shown in the inset 1 in Figure 2b), indicative of the π−π interactions between DBSA and GFs [13]. FT-IR spectra of pristine GFs (Figure 2c) present no peak because of the absence of functional groups. The broad band at ~3400 cm^{-1}, an indication of the stretching vibration of O−H bonds, is weak in PEDOT:PSS possibly because of the steric hindrance effect arising from the large benzene rings in PSS chains.

Compared with neat PEDOT:PSS, the peak of O−H bonds for GF/PEDOT:PSS composites were intensified and showed an obvious downshift, which indicated the formation of hydrogen bonds between DBSA and PEDOT:PSS. Therefore, interfacial interactions among components in composites are summarized as the π−π stacking between GFs and DBSA, and the hydrogen bonds between DBSA and PEDOT:PSS, as illustrated in Figure 2d.

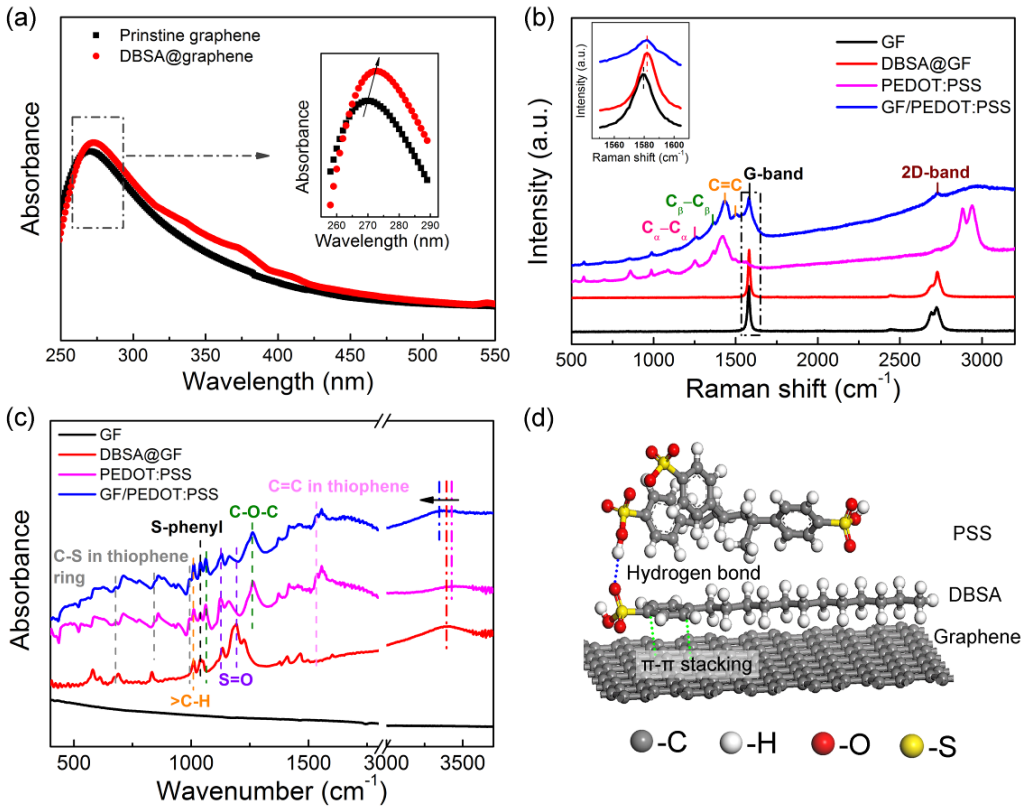

Figure 2: (a) UV−vis spectra of graphene with and without the DBSA functionalization; (b) Raman spectra and (c) FT-IR spectra of different materials; and (d) schematics of the proposed mechanisms for interfacial interactions among different components of composites (the PEDOT chains are omitted for a clearer illustration). Insets in (a,b) show the enlarged spectra of the emphasized areas.

3.2 Densities and Electrical Conductivities of GF/PEDOT:PSS Composites

The pristine freestanding GFs showed an ultralow apparent density of 9.29×10^{-3} g/cm^3 and an extremely high porosity of 99.6% (Figure 3a). The apparent density increased, while the porosity underwent a gradual decrease with the increasing PEDOT:PSS coating. Attributed to the highly conductive polymer coating, electrical conductivities of composites were significantly improved (Figure 3b), achieving a largest value of 43.2 S/cm by GF/PEDOT:PSS-7. Mechanisms for the greatly enhanced electrical conductivities were analyzed by studying the morphology changes of GFs after the coating of PEDOT:PSS on both nanoscopic and microscopic scale. On the nanoscopic scale, the applied PEDOT:PSS coating bridged resistive grain boundaries of GFs (Figure 1b,c), providing more conductive paths for electrons. The microscopic effect referred to the gradual changes in the porous structure of composites with the increasing PEDOT:PSS coatings. As shown in Figure 3c, large openings between the skeleton of GFs were connected by the polymer coating, leading to enhanced conductive networks. Pores among graphene tubes were connected (Figure 3c,d) and the thickness of polymer coating increased (insets in Figure 3d) gradually with the increasing amount of PEDOT:PSS coating. The percent of connected pores enhanced from ~36% to almost 100% when the mass ratio of PEDOT:PSS to GFs was increased from 3.5 to 7.0, see inset of Figure 3b. After the complete

connection of pores, further increment in polymer coating resulted in a marginal reduction in electrical conductivities because of the saturation and relatively lower electrical conductivity of PEDOT:PSS than graphene.

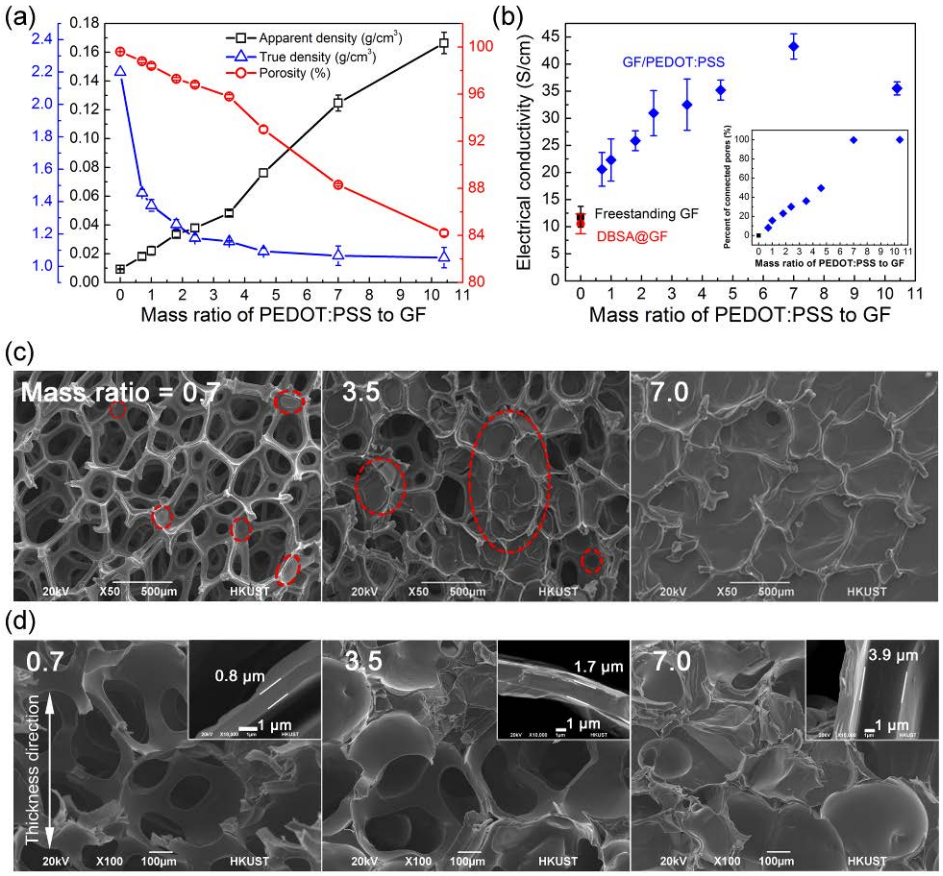

Figure 3: (a) Densities and porosities and (b) electrical conductivities of composites as a function of PEDOT:PSS-to-GF mass ratio; and SEM images of (c) surfaces and (d) freeze-fractured cross-sections of GF/PEDOT:PSS composites with PEDOT:PSS-to-GF mass ratio of 0.7, 3.5, and 7.0. Inset in (b) shows the percent of connected pores in composites. Red ellipses in (c) are connected pores by the PEDOT:PSS films. Insets in (d) shows the thickness of polymer coatings on the skeleton of GFs.

3.3 EMI Shielding Properties of Composites

Three mechanisms are responsible for EMI shielding, namely reflection (SE_R), absorption (SE_A) and multiple reflection of EM waves [14]. The reflection of EM waves is determined by interactions between the incident waves and free charges on material surfaces [15]. In general, the higher the electrical conductivity and the higher the free charge carrier concentration, the higher the SE_R. The SE_A is related to the capability of shielding materials to attenuate EM radiations to thermal and internal energies [15]. The processes that promote energy consumption and dissipation, such as the formation of continuous thermal/electrical conductive paths, the generation of localized current and the enhancement of polarization/relaxation, are beneficial to SE_A. When the total SE_T of a material is higher than 10 dB, almost all multiple-reflected radiations are further attenuated by absorption. Therefore, both the directly absorbed and multiple-reflected EM waves contribute to SE_A of shielding materials.

The EMI shielding properties of GF/PEDOT:PSS composites with different mass ratios of PEDOT:PSS to GF are shown in Figure 4. The SE_A of composites enhanced gradually when the mass ratio increased from 1 to 4.6, whereas SE_R fluctuated at ~10 dB and had a negligible change (Figure 4a). With an electrical conductivity of 22.3 S/cm, GF/PEDOT:PSS-1 showed an average EMI SE_T of

69.1 dB, while GF/PEDOT:PSS-4.6 possessing a larger electrical conductivity of 35.2 S/cm had a higher average SE_T of 91.9 dB (Figure 4b,c). The SE_A contributed over 80% of the total SE_T of composites, exhibiting an absorption dominated EMI shielding behaviour. Thanks to the ultralow densities ranging from 0.0221 to 0.0762 g/cm^3 when the PEDOT:PSS-to-GF mass ratio increased from 1 to 4.6, the composites achieved extraordinary SSEs (Figure 4c). Extremely high SSEs in the ranges of 1206−3124 dB·cm^3/g and 8040−20 800 dB·cm^2/g were obtained when normalized by volumetric and area densities, respectively.

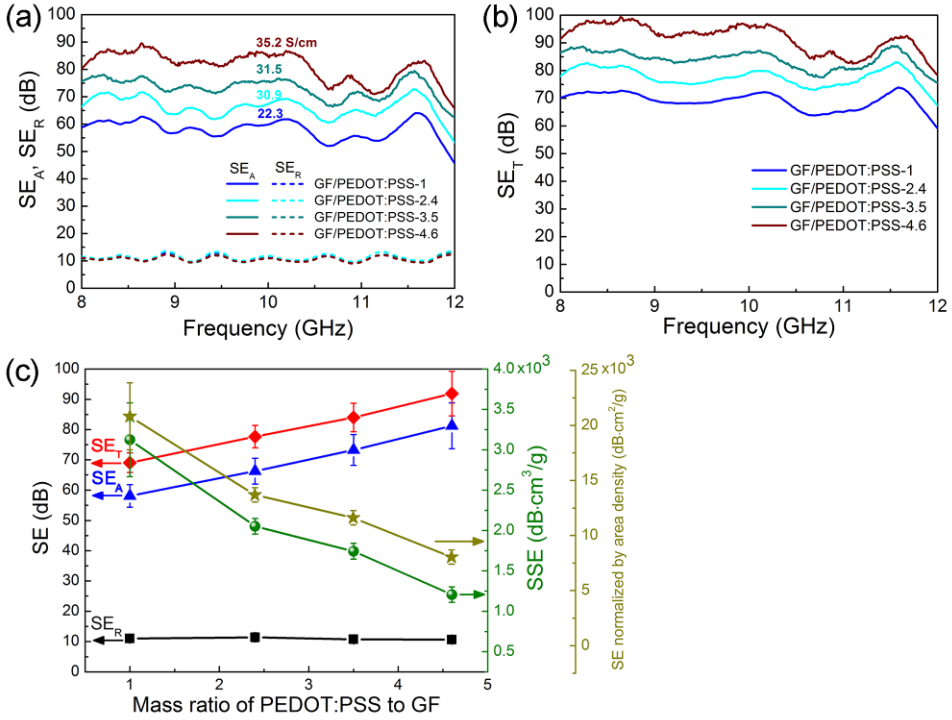

Figure 4: EMI shielding performances of GF/PEDOT:PSS composites: (a) SE_A and SE_R, (b) SE_T as a function of frequency, and (c) summary of SEs and SSEs normalized by volumetric and area densities as a function of PEDOT:PSS-to-GF mass ratio.

Permittivity (ε) and permeability (μ) of composites were specifically studied to understand the mechanisms of excellent EMI shielding performance. The permittivity of composites increased with increasing polymer coating due to the enhancement of dipolar polarization in PEDOT:PSS layers, contributing to higher SE_A values. As shown in Figure 5a-c, negative permittivity and permeability are shown for the GF/PEDOT:PSS composites, suggesting that polarized charges upon the application of EM waves were delocalized on a macroscopic scale rather than aggregated at interfaces [16]. The three-dimensionally interconnected conductive networks and the highly conductive polymer coating are responsible for the effective charge delocalization [16]. The refractive index (n) determined by $n = \pm(\varepsilon\mu)^{1/2}$ is related to the sign of permittivity and permeability. With negative permittivity and permeability, the GF/PEODT:PSS composites had an negative refractive index, which is defined as the left-handed material (Figure 5d) [17]. With absolute values of permittivity larger than 1, incident EM radiations cannot propagate inside the lossy left-handed GF/PEDOT:PSS composites. In other words, waves are effectively absorbed, leading to large SE_A with few transmitted waves.

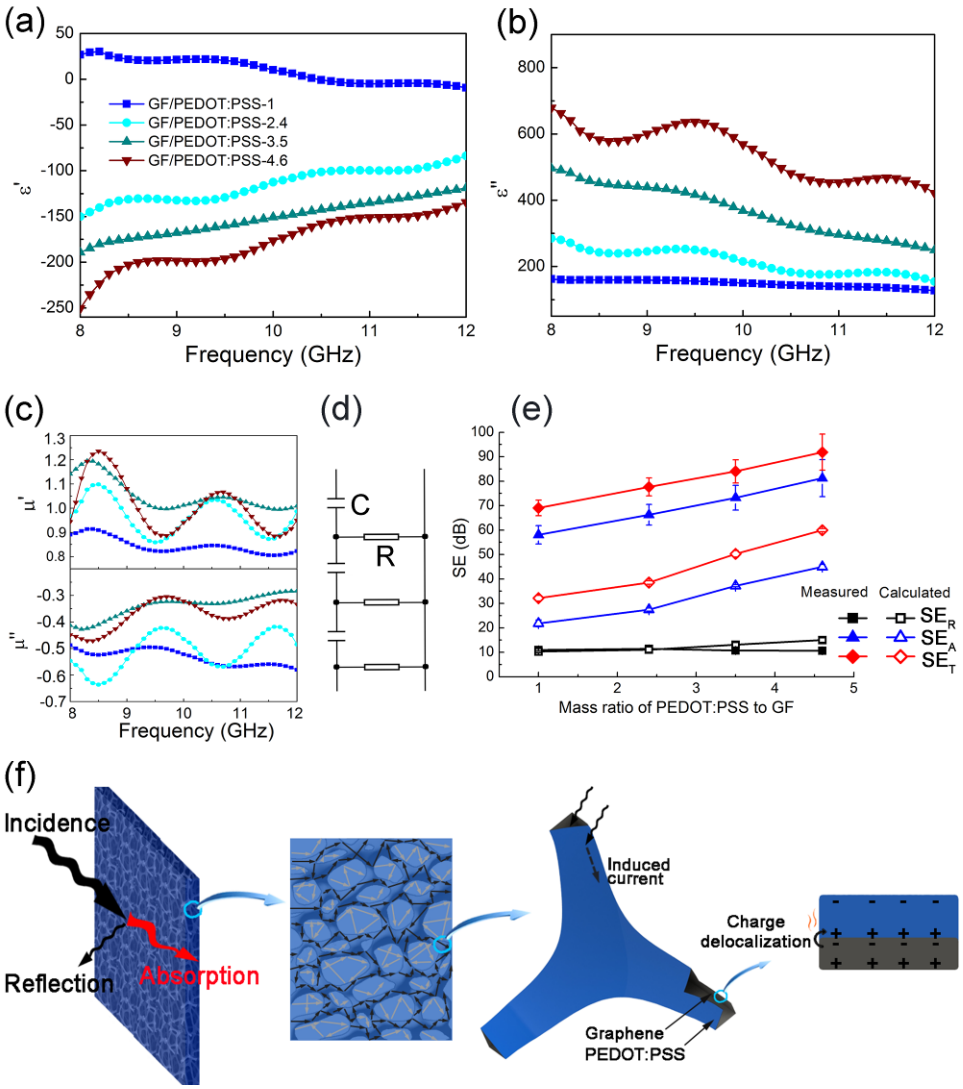

Figure 5: (a) Real, (b) imaginary parts of permittivity and (c) permeability of GF/PEDOT:PSS composites; (d) the equivalent circuit of left-handed materials; (e) comparison of measured and calculated EMI SEs of composites; and (f) summary of EMI shielding mechanisms for GF/PEDOT:PSS composites.

Considering the highly conductive nature of GF/PEDOT:PSS composites, SE_R and SE_A are calculated by Eq (5,6) which are usually used for the prediction of SEs of solid conductive materials [18]:

$$SE_R = 10\log\left(\frac{\sigma_{ac}}{32\pi f\varepsilon_0\mu'}\right) \tag{5}$$

$$SE_A = 8.68t\sqrt{\sigma_{ac}\pi f\mu_0\mu'} \tag{6}$$

where μ_0, μ' and t are the vacuum permeability (1.257×10^{-6} H/m), the real permeability and the sample thickness, respectively. The alternative electrical conductivity σ_{ac} is obtained by $\sigma_{ac}=2\pi f\varepsilon_0\varepsilon''$, where ε_0 and ε'' are the vacuum permittivity (8.854×10^{-12} F/m) and the imaginary permittivity of materials, respectively. The comparison between experimental and theoretical SEs are plotted in Figure 5e. The measured and calculated SE_R agree well because the SE_R is related to the interaction between incident waves and free charges on materials' surfaces and is not dependent on morphological features. However, the experimental SE_A are always larger, by over 35 dB, than the theoretical values. This is

because Eq 6 only takes materials properties in consideration, while other parameters − such as morphological characterizations (porosity and cellularity), charge delocalization, EM wave induced local current, and multiple reflection within and between hollow graphene tubes of GFs − also contribute to SE_A.

The EMI shielding properties of GF/PEDOT:PSS composites are compared with different carbon-based materials reported in the literature, as plotted in Figure 6. Solid materials show moderate EMI SEs in the range of 20-60 dB but low SSEs resulted from relatively high densities. Porous materials with lower densities of generally smaller than 0.5 g/cm^3 have compatible SEs with solid composites, while their SSEs outperformed the counterpart. Exceptional EMI SEs varied in the range of 65-91.9 dB were achieved by GF/PEDOT:PSS composites at ultralow densities of 0.022-0.076 g/cm^3 in this study. This finding makes GF/PEDOT:PSS composites applicable for applications where lightweight is important, such as aerospace structures and portable devices.

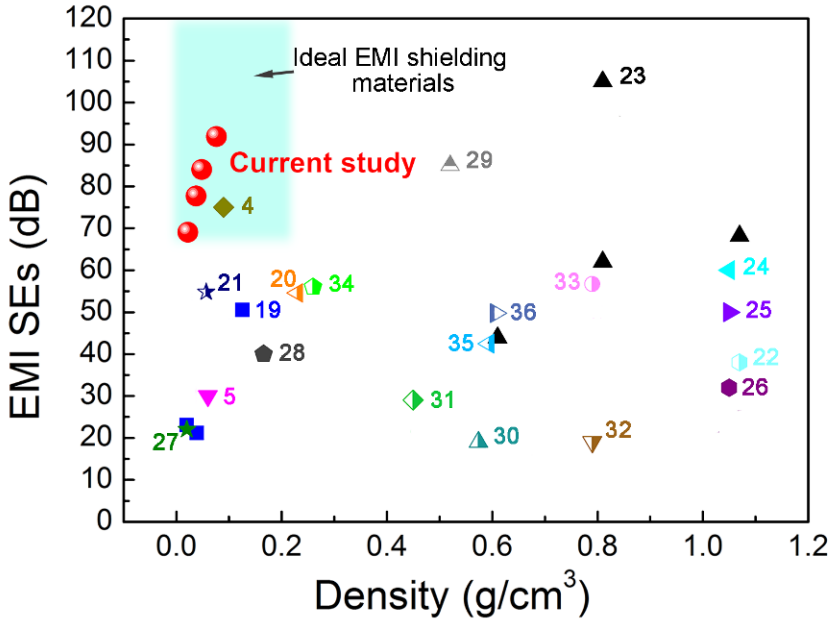

Figure 6. Comparison of EMI SEs of different carbon-based materials: porous CNT/GF/PDMS [4]; porous GF/PDMS [5]; multiwall carbon nanotubes (MWCNT)/waterborne polyurethane (WPU) aerogels [19]; CuNi/carbon nanotubes (CNTs) foam [20]; graphene oxide (GO)/cellulose aerogels[21]; aligned reduced GO/epoxy [22]; CVD fabricated graphene papers [23]; MWCNT/ polystyrene (PS) [24]; MWCNT/acrylonitrile-butadiene-styrene [25]; graphene/WPU [26]; CNT sponge [27]; commercial carbon foam [28]; MWCNTs decorated carbon foam [29]; CNT/PS foam [30]; porous graphene/PS [31]; graphene/poly(methyl methacrylate) foam [32]; porous MWCNT/PVDF [33]; MWCNT-based mesocarbon microbead composite paper [34]; silicon carbide nanowires/carbon foam [35]; carbon foams [36].

4 CONCLUSION

A novel and facile approach was developed for the fabrication of ultra-lightweight GF/PEDOT:PSS composites by drop coating of PEDOT:PSS solutions onto DBSA functionalized freestanding GFs. Large electrical conductivities and extremely high EMI shielding properties were obtained. Mechanisms for EMI shielding were analysed based on both experimental results and theoretical calculations. A summary is made in following:

(i) The wettability between GFs and PEDOT:PSS was significantly improved by the noncovalent functionalization using DBSA. The π–π stacking formed between GFs and DBSA, while hydrogen bonds were introduced between DBSA and PEDOT:PSS. Attributed to the enhanced interfacial

interactions between composite constituents, uniform porous GF/PEDOT:PSS composites were fabricated.

(ii) The apparent densities of GF/PEDOT:PSS composites increased gradually from 0.0182 to 0.1664 g/cm^3 while the porosities underwent a decrease from 98.8 to 84.2% when the mass ratio of PEDOT:PSS to GF was increased from 0.7 to 11.4. A maximum electrical conductivity of 43.2 S/cm were resulted from both the bridging of resistive grain boundaries and the connection of large openings among cellular skeletons of GFs by the conductive polymer coating.

(iii) Extraordinary EMI SEs, SSEs, and SEs normalized by area densities in the range of 65-91.9 dB, 1206−3124 dB·cm^2/g and 8040−20 800 dB·cm^2/g, respectively, were delivered by composites in this study. The large electrical conductivities, the effective charge delocalization, and the porous structure are mainly responsible for the absorption-dominated EMI shielding.

ACKNOWLEDGEMENTS

This project was financially supported by the Research Grants Council of Hong Kong SAR (GRF Projects: 16203415 and 16229216). Technical assistance from the Advanced Engineering Material Facility and the Materials Characterization and Preparation Facilities at HKUST, and Applied Electromagnetics Laboratory at City University of Hong Kong is also appreciated.

REFERENCES

[1] Y. Wu, Z. Wang, X. Liu, X. Shen, Q. Zheng, Q. Xue and J.-K. Kim, Ultralight graphene foam/conductive polymer composites for exceptional electromagnetic interference shielding, *ACS Applied Materials & Interfaces*, **9**, 2017, pp. 9059-9069.

[2] S. Geetha, K.K. Satheesh Kumar, C.R.K. Rao, M. Vijayan and D.C. Trivedi, EMI shielding: methods and materials—A review, *Journal of Applied Polymer Science*, **112**, 2009, pp. 2073-2086.

[3] N. Toshima, K. Oshima, H. Anno, T. Nishinaka, S. Ichikawa, A. Iwata and Y. Shiraishi, Novel hybrid organic thermoelectric materials: Three-component hybrid films consisting of a nanoparticle polymer complex, carbon nanotubes, and vinyl polymer, *Advanced Materials*, **27**, 2015, pp. 2246-2251.

[4] X. Sun, X. Liu, X. Shen, Y. Wu, Z. Wang and J.-K. Kim, Graphene foam/carbon nanotube/poly(dimethyl siloxane) composites for exceptional microwave shielding, *Composites Part A: Applied Science and Manufacturing*, **85**, 2016, pp. 199-206.

[5] Z. Chen, C. Xu, C. Ma, W. Ren and H.-M. Cheng, Lightweight and flexible graphene foam composites for high-performance electromagnetic interference shielding, *Advanced Materials*, **25**, 2013, pp. 1296-1300.

[6] Z. Zeng, M. Chen, H. Jin, W. Li, X. Xue, L. Zhou, Y. Pei, H. Zhang and Z. Zhang, Thin and flexible multi-walled carbon nanotube/waterborne polyurethane composites with high-performance electromagnetic interference shielding, *Carbon*, **96**, 2016, pp. 768-777.

[7] X.-H. Li, X. Li, K.-N. Liao, P. Min, T. Liu, A. Dasari and Z.-Z. Yu, Thermally annealed anisotropic graphene aerogels and their electrically conductive epoxy composites with excellent electromagnetic interference shielding efficiencies, *ACS Applied Materials & Interfaces*, **8**, 2016, pp. 33230-33239.

[8] P. Saini, V. Choudhary, B. Singh, R. Mathur and S. Dhawan, Enhanced microwave absorption behavior of polyaniline-CNT/polystyrene blend in 12.4–18.0 GHz range, *Synthetic Metals*, **161**, 2011, pp. 1522-1526.

[9] M. Kim, H. Kim, S. Byun, S. Jeong, Y. Hong, J. Joo, K. Song, J. Kim, C. Lee and J. Lee, PET fabric/polypyrrole composite with high electrical conductivity for EMI shielding, *Synthetic Metals*, **126**, 2002, pp. 233-239.

[10] X. Zhang, Y. Huang and P. Liu, Enhanced electromagnetic wave absorption properties of poly(3, 4-ethylenedioxythiophene) nanofiber-decorated graphene sheets by non-covalent interactions, *Nano-Micro Letters*, **8**, 2016, pp. 131-136.

[11] J. Jia, X. Sun, X. Lin, X. Shen, Y.-W. Mai and J.-K. Kim, Exceptional electrical conductivity and fracture resistance of 3D interconnected graphene foam/epoxy composites, *ACS Nano*, **8**, 2014, pp. 5774-5783.
[12] X. Liu, X. Sun, Z. Wang, X. Shen, Y. Wu and J.-K. Kim, Planar porous graphene woven fabric/epoxy composites with exceptional electrical, mechanical properties, and fracture toughness, *ACS Applied Materials & Interfaces*, **7**, 2015, pp. 21455-21464.
[13] Z. Wang, X. Shen, M. Akbari Garakani, X. Lin, Y. Wu, X. Liu, X. Sun and J.K. Kim, Graphene aerogel/epoxy composites with exceptional anisotropic structure and properties, *ACS Applied Materials & Interfaces*, **7**, 2015, pp. 5538-5549.
[14] N. Li, Y. Huang, F. Du, X. He, X. Lin, H. Gao, Y. Ma, F. Li, Y. Chen and P.C. Eklund, Electromagnetic interference (EMI) shielding of single-walled carbon nanotube epoxy composites, *Nano Letters*, **6**, 2006, pp. 1141-1145.
[15] W.-L. Song, M.-S. Cao, M.-M. Lu, S. Bi, C.-Y. Wang, J. Liu, J. Yuan and L.-Z. Fan, Flexible graphene/polymer composite films in sandwich structures for effective electromagnetic interference shielding, *Carbon*, **66**, 2014, pp. 67-76.
[16] X. Zhang, S. Wei, N. Haldolaarachchige, H.A. Colorado, Z. Luo, D.P. Young and Z. Guo, Magnetoresistive conductive polyaniline–barium titanate nanocomposites with negative permittivity, *The Journal of Physical Chemistry C*, **116**, 2012, pp. 15731-15740.
[17] D.R. Smith and N. Kroll, Negative refractive index in left-handed materials, *Physical Review Letters*, **85**, 2000, pp. 2933.
[18] K. Singh, A. Ohlan, V.H. Pham, R. Balasubramaniyan, S. Varshney, J. Jang, S.H. Hur, W.M. Choi, M. Kumar and S. Dhawan, Nanostructured graphene/Fe_3O_4 incorporated polyaniline as a high performance shield against electromagnetic pollution, *Nanoscale*, **5**, 2013, pp. 2411-2420.
[19] Z. Zeng, H. Jin, M. Chen, W. Li, L. Zhou and Z. Zhang, Lightweight and anisotropic porous MWCNT/WPU composites for ultrahigh performance electromagnetic interference shielding, *Advanced Functional Materials*, **26**, 2016, pp. 303-310.
[20] K. Ji, H. Zhao, J. Zhang, J. Chen and Z. Dai, Fabrication and electromagnetic interference shielding performance of open-cell foam of a Cu–Ni alloy integrated with CNTs, *Applied Surface Science*, **311**, 2014, pp. 351-356.
[21] C. Wan and J. Li, Graphene oxide/cellulose aerogels nanocomposite: Preparation, pyrolysis, and application for electromagnetic interference shielding, *Carbohydrate Polymers*, **150**, 2016, pp. 172-179.
[22] N. Yousefi, X. Sun, X. Lin, X. Shen, J. Jia, B. Zhang, B. Tang, M. Chan and J.-K. Kim, Highly aligned graphene/polymer nanocomposites with excellent dielectric properties for high-performance electromagnetic interference shielding, *Advanced Materials*, **26**, 2014, pp. 5480-5487.
[23] L. Zhang, N.T. Alvarez, M. Zhang, M. Haase, R. Malik, D. Mast and V. Shanov, Preparation and characterization of graphene paper for electromagnetic interference shielding, *Carbon*, **82**, 2015, pp. 353-359.
[24] M. Arjmand, T. Apperley, M. Okoniewski and U. Sundararaj, Comparative study of electromagnetic interference shielding properties of injection molded versus compression molded multi-walled carbon nanotube/polystyrene composites, *Carbon*, **50**, 2012, pp. 5126-5134.
[25] M.H. Al-Saleh, W.H. Saadeh and U. Sundararaj, EMI shielding effectiveness of carbon based nanostructured polymeric materials: A comparative study, *Carbon*, **60**, 2013, pp. 146-156.
[26] S.-T. Hsiao, C.-C.M. Ma, H.-W. Tien, W.-H. Liao, Y.-S. Wang, S.-M. Li and Y.-C. Huang, Using a non-covalent modification to prepare a high electromagnetic interference shielding performance graphene nanosheet/water-borne polyurethane composite, *Carbon*, **60**, 2013, pp. 57-66.
[27] M. Crespo, M. González, A.L. Elías, L. Pulickal Rajukumar, J. Baselga, M. Terrones and J. Pozuelo, Ultra-light carbon nanotube sponge as an efficient electromagnetic shielding material in the GHz range, *Physica Status Solidi (RRL)-Rapid Research Letters*, **8**, 2014, pp. 698-704.
[28] F. Moglie, D. Micheli, S. Laurenzi, M. Marchetti and V.M. Primiani, Electromagnetic shielding performance of carbon foams, *Carbon*, **50**, 2012, pp. 1972-1980.

[29] R. Kumar, S.R. Dhakate, T. Gupta, P. Saini, B.P. Singh and R.B. Mathur, Effective improvement of the properties of light weight carbon foam by decoration with multi-wall carbon nanotubes, *Journal of Materials Chemistry A*, **1**, 2013, pp. 5727-5735.
[30] Y. Yang, M.C. Gupta, K.L. Dudley and R.W. Lawrence, Novel carbon nanotube-polystyrene foam composites for electromagnetic interference shielding, *Nano Letters*, **5**, 2005, pp. 2131-2134.
[31] D.-X. Yan, P.-G. Ren, H. Pang, Q. Fu, M.-B. Yang and Z.-M. Li, Efficient electromagnetic interference shielding of lightweight graphene/polystyrene composite, *Journal of Materials Chemistry*, **22**, 2012, pp. 18772-18774.
[32] H.-B. Zhang, Q. Yan, W.-G. Zheng, Z. He and Z.-Z. Yu, Tough graphene−polymer microcellular foams for electromagnetic interference shielding, *ACS Applied Materials & Interfaces*, **3**, 2011, pp. 918-924.
[33] H. Wang, K. Zheng, X. Zhang, X. Ding, Z. Zhang, C. Bao, L. Guo, L. Chen and X. Tian, 3D network porous polymeric composites with outstanding electromagnetic interference shielding, *Composites Science and Technology*, **125**, 2016, pp. 22-29.
[34] A. Chaudhary, S. Kumari, R. Kumar, S. Teotia, B.P. Singh, A.P. Singh, S. Dhawan and S.R. Dhakate, Lightweight and easily foldable MCMB-MWCNTs composite paper with exceptional electromagnetic interference shielding, *ACS Applied Materials & Interfaces*, **8**, 2016, pp. 10600-10608.
[35] S. Farhan, R. Wang and K. Li, Electromagnetic interference shielding effectiveness of carbon foam containing in situ grown silicon carbide nanowires, *Ceramics International*, **42**, 2016, pp. 11330-11340.
[36] Y. Li, B. Shen, X. Pei, Y. Zhang, D. Yi, W. Zhai, L. Zhang, X. Wei and W. Zheng, Ultrathin carbon foams for effective electromagnetic interference shielding, *Carbon*, **100**, 2016, pp. 375-385.